Journal of Sound and Vibration 329 (2010) 302–316

Contents lists available at ScienceDirect

Journal of Sound and Vibration

journal homepage: www.elsevier.com/locate/jsvi

# Hybrid finite element method applied to supersonic flutter of an empty or partially liquid-filled truncated conical shell

Farhad Sabri, Aouni A. Lakis *

*Department of Mechanical Engineering, Ecole Polytechnique de Montreal, C.P. 6079 Succursale Centre-ville, Montréal, Canada H3C 3A7*

ARTICLE INFO

*Article history:*
Received 9 April 2009
Received in revised form
17 September 2009
Accepted 18 September 2009
Handling Editor: H. Ouyang

ABSTRACT

In this study, aeroelastic analysis of a truncated conical shell subjected to the external supersonic airflow is carried out. The structural model is based on a combination of linear Sanders thin shell theory and the classic finite element method. Linearized first-order potential (piston) theory with the curvature correction term is coupled with the structural model to account for pressure loading. The influence of stress stiffening due to internal or external pressure and axial compression is also taken into account. The fluid-filled effect is considered as a velocity potential variable at each node of the shell elements at the fluid–structure interface in terms of nodal elastic displacements. Aeroelastic equations using the hybrid finite element formulation are derived and solved numerically. The results are validated using numerical and theoretical data available in the literature. The analysis is accomplished for conical shells of different boundary conditions and cone angles. In all cases the conical shell loses its stability through coupled-mode flutter. This proposed hybrid finite element method can be used efficiently for design and analysis of conical shells employed in high speed aircraft structures.



## 1. Introduction

Shells of revolution, particularly conical shells are one of the primary structural elements in high speed aircraft. Their applications include the propellant tank or gas-deployed skirt of spacecrafts. Due to the large expanses in their geometry combined with thin wall thicknesses, conical shells are more susceptible to dynamic instability or flutter induced by high-Mach number gas flow. It is therefore important to understand the effect of different parameters and loadings on their dynamic response.

Aeroelastic analysis of shells and plates has been investigated by numerous researchers experimentally and analytically [1]. Dowell addressed a comprehensive study of the aeroelasticity of shells and plates in his book [2]. Aeroelasticity of circular cylindrical shells has also been reported in detail by different researchers [3–9], while less information is available for conical shells. During the 1970s some researchers focused their efforts on conical shell aeroelasticity. The earliest work in this field was found by Shulman [10]. Ueda, Kobayashi and Kihira [11] investigated theoretically and experimentally the supersonic flutter of a conical shell. Dixon and Hudson [12] studied the flutter and vibration of an orthotropic conical shell theoretically. Miserentino and Dixon [13] investigated experimentally the vibration and flutter of a pressurized truncated conical shell. Bismarck-Nasr and Costa-Savio [14] found a finite element solution for the supersonic flutter of conical shells. Sunder, Ramakrishnan and Sengupta [15] reported the success of the application of finite element analysis to calculate the flutter of a laminated conical shell. In another study they found the optimum cone angle in aeroelastic flutter [16]. Mason and Blotter [17] used a finite element technique to find the flutter boundary for a conical shell (a typical rocket nozzle

* Corresponding author. Tel.: +1 514 340 4711; fax: +1 514 340 4172.
*E-mail address:* aouni.lakis@polymtl.ca (A.A. Lakis).

0022-460X/$ - see front matter © 2009 Elsevier Ltd. All rights reserved.
doi:10.1016/j.jsv.2009.09.023

element) subjected to an internal supersonic gas flow. Most of these works considered only simply supported conical shells. Not all boundary conditions were satisfied by these methods [17]. There are also other researchers who focused on the dynamic stability and fluid–structure interaction of conical shells. For example, Lakis, Van Dyke and Ouriche [18] investigated the dynamic analysis of anisotropic fluid-filled conical shells. Recently, Kumar and Ganesan [19] studied the vibration of conical shells conveying fluid.

For such a problem, use of an analytical approach becomes very complicated if one wishes to include complex structures, boundary conditions, material and loading. Therefore, numerical methods such as the finite element method (FEM) are powerful tools for cases involving changes to all factors affecting flutter boundaries.

The objective of the present study is to develop a general hybrid finite element package for predicting the aeroelastic behavior of isotropic conical shells with boundary conditions which can be varied as desired. The solution scheme is based on the finite element development done by Lakis et al. [18] for conical shells and Lakis and Paidoussis [20] for cylindrical shells. These developed methods demonstrated precise and fast convergence with few numerical difficulties. The element is a conical frustum instead of the usual rectangular shell element. Sanders linear thin shell theory where all strains vanish for rigid body motions (other theories are incapable of this attribute) is coupled with linearized first order piston theory. In the case of a fluid-filled shell the effect of dynamic pressure acting on the wall is modeled based on a velocity potential formulation and Bernoulli's equation. It is assumed that the fluid is incompressible and has no free-surface effect. Initial stress stiffening in the presence of shell internal or external pressure and axial compression is also applied in the formulation. Finally the linear mass, damping and stiffness matrices are obtained. The aeroelastic equation of motion is driven out to a standard eigenvalue problem. The flutter boundary is found by tracking the real and imaginary parts of the eigenvalues as dynamic pressure is varied.

## 2. Finite element formulation

### 2.1. Structural modeling

Sanders [21] developed an improved thin shell theory based on Love's first approximation. One advantage of Sanders theory is that all strains vanish for small rigid-body motion. In this study the structure is modeled using hybrid finite element method which is a combination of Sanders shell theory and classic finite element. In this hybrid method, the displacement functions are found from exact solution of Sanders shell theory rather than approximated by polynomial functions done in classic finite element method. According to the Sanders linear thin shell theory the equilibrium equations for a conical shell (Fig. 1) are written as:

$$
\begin{aligned}
r\frac{\partial N_x}{\partial x}+N_x\sin\alpha+\frac{\partial N_{x\theta}}{\partial\theta}-N_\theta\sin\alpha-\frac{\cos\alpha}{2r}\frac{\partial M_{x\theta}}{\partial\theta}&=0\\
r\frac{\partial N_{x\theta}}{\partial x}+2N_{x\theta}\sin\alpha+\frac{\partial N_\theta}{\partial\theta}+\frac{3}{2}\cos\alpha\frac{\partial M_{x\theta}}{\partial\theta}-\frac{3}{4}\frac{\sin 2\alpha}{r}M_{x\theta}+\frac{\cos\alpha}{r}\frac{\partial M_\theta}{\partial\theta}&=0\\
r\frac{\partial^2 M_x}{\partial x^2}+2\sin\alpha\frac{\partial M_x}{\partial x}+2\frac{\partial^2 M_{x\theta}}{\partial x\partial\theta}+2\frac{\sin\alpha}{r}\frac{\partial M_{x\theta}}{\partial\theta}+\frac{1}{r}\frac{\partial^2 M_\theta}{\partial\theta^2}-\sin\alpha\frac{\partial M_\theta}{\partial x}-N_\theta\cos\alpha&=0
\end{aligned}
\tag{1}
$$

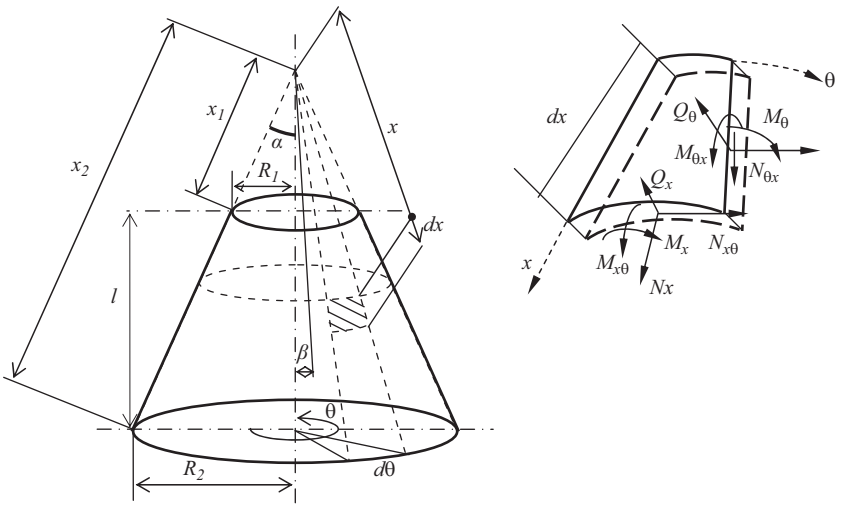


**Fig. 1.** Geometry of a truncated conical shell.

where $N$ and $M$ are the stress resultant and stress couples, respectively. The strain-displacement equations for three infinitesimal displacements in axial $U$, radial $W$, and circumferential $V$ directions are [21]:

$$\begin{Bmatrix} \varepsilon_x \\ \varepsilon_\theta \\ 2\overline{\varepsilon}_{x\theta} \\ \kappa_x \\ \kappa_\theta \\ \overline{\kappa}_{x\theta} \end{Bmatrix} = \begin{Bmatrix} \dfrac{\partial U}{\partial x} \\ \dfrac{1}{x\sin\alpha}\dfrac{\partial V}{\partial \theta} + \dfrac{U}{x} + \dfrac{W\cot\alpha}{x} \\ \dfrac{\partial V}{\partial x} + \dfrac{1}{x\sin\alpha}\dfrac{\partial U}{\partial \theta} - \dfrac{V}{x} \\ -\dfrac{\partial^2 W}{\partial x^2} \\ \dfrac{\partial V}{\partial \theta}\dfrac{\cos\alpha}{x^2\sin^2\alpha} - \dfrac{1}{x^2\sin^2\alpha}\dfrac{\partial^2 W}{\partial \theta^2} - \dfrac{\partial W}{\partial x}\dfrac{1}{x} \\ -\dfrac{2}{x\sin\alpha}\dfrac{\partial^2 W}{\partial x\partial\theta} + \dfrac{3}{2}\dfrac{\cot\alpha}{x}\dfrac{\partial V}{\partial x} - \dfrac{\partial U}{\partial \theta}\dfrac{\cos\alpha}{2x^2\sin^2\alpha} + \dfrac{2\sin\alpha}{x^2\sin^2\alpha}\dfrac{\partial W}{\partial \theta} - \dfrac{3}{2}\dfrac{\cot\alpha}{x^2}V \end{Bmatrix} \tag{2}$$

Displacements $U$, $W$ and $V$ in the global Cartesian coordinate system are related to displacements $U_i$, $W_i$, $V_i$ indicated in Fig. 2 by:

$$\begin{Bmatrix} U \\ W \\ V \end{Bmatrix} = \begin{bmatrix} \cos\alpha & \sin\alpha & 0 \\ -\sin\alpha & \cos\alpha & 0 \\ 0 & 0 & 1 \end{bmatrix} \begin{Bmatrix} U_i \\ W_i \\ V_i \end{Bmatrix} \tag{3}$$

The stress–strain relation for an anisotropic shell is expressed by:

$$[\sigma] = [p][\varepsilon] \tag{4}$$

where **P** is the elasticity matrix for an anisotropic shell. Upon substitution of Eqs. (2) and (4) into Eq. (1), a system of equilibrium equations can be obtained as a function of displacements:

$$\begin{aligned} L_1(U, W, V, B_{ij}) &= 0 \\ L_2(U, W, V, B_{ij}) &= 0 \\ L_3(U, W, V, B_{ij}) &= 0 \end{aligned} \tag{5}$$

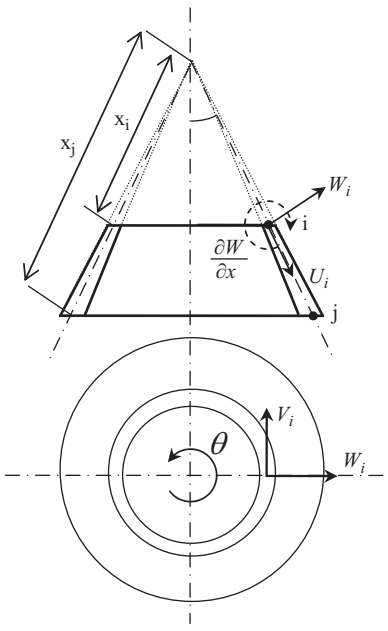


**Fig. 2.** Conical frustum element.

These three linear partial differential operators $L_1$, $L_2$ and $L_3$ are given in the Appendix, and $B_{ij}$ are elements of the elasticity matrix which, for an isotropic thin shell with thickness $h$ are given by:

$$[p] = \begin{bmatrix} D & \upsilon D & 0 & 0 & 0 & 0 \\ \upsilon D & D & 0 & 0 & 0 & 0 \\ 0 & 0 & \dfrac{D(1-\upsilon)}{2} & 0 & 0 & 0 \\ 0 & 0 & 0 & K & \upsilon K & 0 \\ 0 & 0 & 0 & \upsilon K & K & 0 \\ 0 & 0 & 0 & 0 & 0 & \dfrac{K(1-\upsilon)}{2} \end{bmatrix} \tag{6}$$

where

$$K = \frac{Eh^3}{12(1-\upsilon^2)} D = \frac{Eh}{1-\upsilon^2} \tag{7}$$

The element is a circumferential conical frustum shown in Fig. 2. It has two nodal circles with four degrees of freedom; axial, radial, circumferential and rotation at each node. This element type makes it possible to use thin shell equations easily to find the exact solution of displacement functions rather than an approximation with polynomial functions as is done in classic FEM. The displacement functions for $n$th circumferential wave number in Fourier series form can be written as:

$$\begin{aligned} U(r,x,\theta) &= \sum_{n=0}^{\infty} u(x)\cos(n\theta) \\ W(r,x,\theta) &= \sum_{n=0}^{\infty} w(x)\cos(n\theta) \\ V(r,x,\theta) &= \sum_{n=0}^{\infty} v(x)\sin(n\theta) \end{aligned} \tag{8}$$

The solutions for the magnitude of displacements can have the following form [22]:

$$\begin{Bmatrix} u(x) \\ v(x) \\ w(x) \end{Bmatrix} = \left(\frac{x}{l}\right)^{(\lambda-1)/2} \begin{Bmatrix} A \\ B \\ C \end{Bmatrix} \tag{9}$$

where $\lambda$, $A$, $B$ and $C$ are complex numbers and $l$ is an arbitrary reference length. By replacing Eqs. (8) and (9) into Eqs. (5), three ordinary homogeneous differential equations in the following form are obtained:

$$\begin{bmatrix} H_{11} & H_{12} & H_{13} \\ H_{21} & H_{22} & H_{23} \\ H_{31} & H_{32} & H_{33} \end{bmatrix} \begin{Bmatrix} A \\ B \\ C \end{Bmatrix} = \begin{Bmatrix} 0 \\ 0 \\ 0 \end{Bmatrix} \tag{10}$$

In order to have a non-trivial solution the determinant of the above system of equations must be equal to zero. Application of this condition yields the following characteristic equation:

$$h_8\lambda^8 + h_6\lambda^6 + h_4\lambda^4 + h_2\lambda^2 + h_0 = 0 \tag{11}$$

Each single root of Eq. (11) corresponds to the solution of Eqs. (5). The complete solution is obtained by summation of these roots and constants $A_i$, $B_i$ and $C_i$:

$$\begin{aligned} u(x) &= \sum_{i=1}^{8} A_i y^{\lambda_i - 1} \\ v(x) &= \sum_{i=1}^{8} B_i y^{\lambda_i - 1} \\ w(x) &= \sum_{i=1}^{8} C_i y^{\lambda_i - 1} \end{aligned} \tag{12}$$

where $y$ is the dimensionless ratio given in Eq. (9). The independent constants $A_i$, and $B_i$ can be expressed in terms of $C_i$ and complex numbers $\alpha$ and $\beta$ as:

$$\begin{aligned} A_i &= \alpha_i C_i \\ B_i &= \beta_i C_i \end{aligned} \tag{13}$$

These complex numbers can be obtained by replacing them in Eq. (10) in the following way:

$$\begin{bmatrix} H_{11} & H_{12} \\ H_{21} & H_{22} \end{bmatrix} \begin{Bmatrix} \alpha_i \\ \beta_i \end{Bmatrix} = \begin{Bmatrix} -H_{13} \\ -H_{23} \end{Bmatrix} \tag{14}$$

Finally, the magnitude of displacement functions is written as:

$$\begin{Bmatrix} u(x) \\ w(x) \\ v(x) \end{Bmatrix} = [R]\{C\} \tag{15}$$

The displacement vectors, Eq. (8), that correspond to the circumferential wave number $n$, are written as:

$$\begin{Bmatrix} U(x,\theta) \\ W(x,\theta) \\ V(x,\theta) \end{Bmatrix} = [T][R]\{C\} \tag{16}$$

where matrices **R** can be found in Ref. [18] and **T** are defined as:

$$\begin{bmatrix} \cos n\theta & 0 & 0 \\ 0 & \cos n\theta & 0 \\ 0 & 0 & \sin n\theta \end{bmatrix} \tag{17}$$

The element in Fig. 2 with two nodal lines ($i$ and $j$) and eight degrees of freedom will have the following nodal displacement vector:

$$\begin{Bmatrix} \delta_i \\ \delta_j \end{Bmatrix} = \{U_i, W_i, \partial W_i/\partial x, V_i, U_j, W_j, \partial W_j/\partial x, V_j\}^{\mathrm{T}} = [A]\{C\} \tag{18}$$

where matrix **A** is obtained from the terms of **R**. Now, pre-multiplying Eq. (18) by $\mathbf{A}^{-1}$, the constant vector of $\{C\}$ is found. Eq. (16) can therefore be written in terms of nodal degrees of freedom as:

$$\begin{Bmatrix} U(x,\theta) \\ W(x,\theta) \\ V(x,\theta) \end{Bmatrix} = [T][R][A]^{-1} \begin{Bmatrix} \delta_i \\ \delta_j \end{Bmatrix} = [N] \begin{Bmatrix} \delta_i \\ \delta_j \end{Bmatrix} \tag{19}$$

The strain vector, Eq. (2), will become:

$$\{\varepsilon\} = \begin{bmatrix} [T] & [0] \\ [0] & [T] \end{bmatrix} [Q][A]^{-1}\{\delta\} = [B][\delta] \tag{20}$$

where matrix **Q** can be found in Ref. [18]. This relation can be used to find the stress vector, Eq. (4), in terms of the nodal degrees of freedom vector:

$$\{\sigma\} = [P][B] \begin{Bmatrix} \delta_i \\ \delta_j \end{Bmatrix} \tag{21}$$

Based on the standard finite element formulation [23], the local mass and stiffness matrices are found:

$$\begin{aligned} [m_s] &= \rho h \int\int [N]^{\mathrm{T}}[N] h \, \mathrm{d}A \\ [k_s] &= \int\int [B]^{\mathrm{T}}[P][B] \, \mathrm{d}A \end{aligned} \tag{22}$$

where $\rho$ is the shell density and $\mathrm{d}A = x\sin\alpha \, \mathrm{d}\theta \, \mathrm{d}x$ Finally, the global mass, **M**, and stiffness, **K**, matrices for the entire shell are developed using standard assembling techniques for different boundary conditions.

### 2.2. Stress stiffening

In the presence of initial membrane forces resulting from circumferentially uniform internal or external pressure and axial compression, a strain–energy contribution is introduced into the formulation. It is assumed that the shell is under equilibrium conditions and has not reached its buckling state. The stress resultants of internal pressure, $P_m$, and axial load, $P_x$, (positive in compression) are [12]:

$$\begin{aligned} \overline{N}_\theta &= -xP_m \tan\alpha \\ \overline{N}_x &= -\frac{x}{2} P_m \tan\alpha - \frac{P_x}{2\pi \sin 2\alpha} \\ \overline{N}_{x\theta} &= \overline{N}_{\theta x} = 0 \end{aligned} \tag{23}$$

The potential energy due to this initial strain can be found [24]:

$$U_i = \frac{1}{2}\int\int [\overline{N}_x\phi_{\theta\theta}^2 + \overline{N}_\theta\phi_{xx}^2 + (\overline{N}_x + \overline{N}_\theta)\phi_n^2]\,dA \tag{24}$$

where $\phi_{\theta\theta}$, $\phi_{xx}$ and $\phi_n$ are the strain rotation vectors [21]:

$$\begin{aligned}\phi_{\theta\theta} &= -\frac{\partial W}{\partial x}\\ \phi_{xx} &= \frac{V}{x\tan\alpha} - \frac{1}{x\sin\alpha}\frac{\partial W}{\partial\theta}\\ \phi_n &= \frac{V}{2x} + \frac{1}{2}\frac{\partial V}{\partial x} - \frac{1}{2x\sin\alpha}\frac{\partial U}{\partial\theta}\end{aligned} \tag{25}$$

If the displacements are replaced by Eq. (19) the potential energy in terms of nodal degrees of freedom is generated:

$$U_I = \frac{1}{2}\int_{x_i}^{x_j}\int_0^{2\pi}\{r\}^{\mathrm{T}}\begin{bmatrix}\overline{N}_x & 0 & 0\\ 0 & \overline{N}_\theta & 0\\ 0 & 0 & \overline{N}_x + \overline{N}_\theta\end{bmatrix}\{r\}\,dA \tag{26}$$

where

$$\{r\} = \begin{bmatrix} 0 & -\dfrac{\partial}{\partial x} & 0\\ 0 & -\dfrac{1}{x\sin\alpha}\dfrac{\partial}{\partial\theta} & \dfrac{1}{x\tan\alpha}\\ -\dfrac{1}{2x\sin\alpha}\dfrac{\partial}{\partial\theta} & 0 & \dfrac{1}{2x} + \dfrac{1}{2}\dfrac{\partial}{\partial x}\end{bmatrix}\begin{Bmatrix} U\\ W\\ V\end{Bmatrix} = [\varpi][N]\begin{Bmatrix}\delta_i\\ \delta_j\end{Bmatrix} \tag{27}$$

Therefore, the initial stiffness matrix for each element becomes:

$$[k_I] = \int\int [N]^{\mathrm{T}}[\varpi]^{\mathrm{T}}\begin{bmatrix}\overline{N}_x & 0 & 0\\ 0 & \overline{N}_\theta & 0\\ 0 & 0 & \overline{N}_x + \overline{N}_\theta\end{bmatrix}[\varpi][N]\,dA \tag{28}$$

After assembly, the whole stress stiffness matrix, $\mathbf{K_I}$ is added to the geometry stiffness matrix developed in Eq. (22).

### 2.3. Aerodynamic modeling

Piston theory, introduced by Ashley and Zartarian [25], is a powerful tool for aeroelasticity modeling. In this study the fluid–structure effect due to external pressure loading can be taken into account using linearized first-order potential theory [2]. This pressure is expressed as:

$$P_a = \frac{\gamma p_\infty M^2}{(M^2-1)^{1/2}}\left[\frac{\partial W}{\partial x} + \frac{M^2-2}{M^2-1}\frac{1}{U_\infty}\frac{\partial W}{\partial t} - \frac{W}{2R(M^2-1)^{1/2}}\right] \tag{29}$$

where $P_\infty$, $U_\infty$, $M$ and $\gamma$ are the freestream static pressure, freestream velocity, Mach number and adiabatic exponent of air, respectively. If the Mach number is sufficiently high ($M \geq 2$), and the curvature term, $W/2R(M^2-1)^{1/2}$ is neglected, the result is the so-called piston theory:

$$P_a = -\gamma p_\infty\left[M\frac{\partial W}{\partial x} + \frac{1}{a_\infty}\frac{\partial W}{\partial t}\right] \tag{30}$$

where $a_\infty$ is the freestream speed of sound.

Considering the displacements in Eq. (19), the radial deflection $W$ is:

$$W(x,\theta) = [0\ \ 1\ \ 0][N]\begin{Bmatrix}\delta_i\\ \delta_j\end{Bmatrix} = [N_w]\begin{Bmatrix}\delta_i\\ \delta_j\end{Bmatrix} \tag{31}$$

and the pressure loading, Eq. (29), in terms of nodal degrees of freedom is written as:

$$\begin{aligned}\{P_a\} = \begin{Bmatrix}0\\ p_{radial}\\ 0\end{Bmatrix} &= \frac{-\rho_\infty U_\infty^2}{(M^2-1)^{1/2}}\frac{1}{U_\infty}\left(\frac{M^2-2}{M^2-1}\right)[N_w]\begin{Bmatrix}\dot\delta_i\\ \dot\delta_j\end{Bmatrix}\\ &+ \frac{-\rho_\infty U_\infty^2}{(M^2-1)^{1/2}}\frac{\partial[N_w]}{\partial x}\begin{Bmatrix}\delta_i\\ \delta_j\end{Bmatrix} - \frac{-\rho_\infty U_\infty^2}{(M^2-1)^{1/2}}\left(\frac{1}{2(M^2-1)^{1/2}R_m}\right)[N_w]\begin{Bmatrix}\delta_i\\ \delta_j\end{Bmatrix}\end{aligned} \tag{32}$$

where $\rho_\infty$ is the freestream air density and $R_m$ is the median radius for each element. Based on thermodynamic relations the freestream pressure and velocity can be linked together using the following relation:

$$U_\infty = Ma_\infty$$
$$a_\infty = \sqrt{\gamma \frac{p_\infty}{\rho_\infty}} \tag{33}$$

The general force vector due to a pressure field is written as:

$$\{F_p\} = \int\int [N]^T \{p_a\}\, dA \tag{34}$$

Substituting Eq. (32) into the above relation, the aerodynamic damping, $\mathbf{c_f}$, and stiffness $\mathbf{k_f}$ matrices for each element are obtained:

$$[c_f] = [A^{-1}]^T [D_f][A^{-1}]$$
$$[k_f] = [A^{-1}]^T [G_f][A^{-1}] \tag{35}$$

where

$$[D_f] = \frac{-\rho_\infty U_\infty^2}{(M^2-1)^{1/2}} \frac{1}{U_\infty} \left(\frac{M^2-2}{M^2-1}\right) \int\int [N]^T [N_w]\, dA \tag{36}$$

$$[G_f] = \frac{-\rho_\infty U_\infty^2}{(M^2-1)^{1/2}} \left( \int\int [N]^T \frac{\partial [N_w]}{\partial x} dA - \frac{1}{2(M^2-1)^{1/2} R_m} \int\int [N]^T [N_w]\, dA \right) \tag{37}$$

Finally, global aerodynamic damping, $\mathbf{C_f}$, and aerodynamic stiffness, $\mathbf{K_f}$, matrices are found using assembling procedures.

## 3. Fluid-filled modeling

The Laplace equation satisfied by velocity potential for inviscid, incompressible and irrotational fluid in the conical system is written as [26]:

$$\nabla^2 \varphi = \frac{2}{x}\frac{\partial \varphi}{\partial x} + \frac{\partial^2 \varphi}{\partial x^2} \frac{1}{x^2 (\sin\beta)^2} \frac{\partial^2 \varphi}{\partial \theta^2} + \frac{1}{x^2 \tan\beta} \frac{\partial \varphi}{\partial \beta} + \frac{1}{x^2} \frac{\partial^2 \varphi}{\partial \beta^2} = 0 \tag{38}$$

where, for quiescent fluid ($U_x$=0) the velocity components are:

$$V_\alpha = \frac{1}{x}\frac{\partial \varphi}{\partial \beta} V_\theta = \frac{1}{x \sin\alpha} \frac{\partial \varphi}{\partial \theta} V_x = \frac{\partial \varphi}{\partial x} \tag{39}$$

where $\beta$ is the coordinate along the semivertex angle. Using the Bernoulli equation, hydrodynamic pressure in terms of velocity potential, $\varphi$, and fluid density, $\rho_f$, is found:

$$P_f = \rho_f \frac{\partial \varphi}{\partial t} \tag{40}$$

The impermeability condition, which ensures contact between the shell surface and the peripheral fluid at rest, is written as:

$$V_\alpha = \frac{1}{x}\frac{\partial \varphi}{\partial \beta}\bigg|_{\beta=\alpha} = \frac{\partial W}{\partial t} \tag{41}$$

Method of separation of variables for the velocity potential solution can be done as follows:

$$\varphi(x,\theta,\beta,t) = \sum_{q=1}^{8} R_q(\beta) S_q(x,\theta,t) \tag{42}$$

By placing this relation into the impermeability condition, one can find the function $S_q(x,\theta,t)$ in terms of radial displacement:

$$S_q(x,\theta,t) = \frac{x}{R_q'(\alpha)} \frac{\partial W}{\partial t} \tag{43}$$

With the help of Eq. (43) and substitution of Eq. (42) into Eq. (38), the following second order differential equation in terms of $R_q(\beta)$ is obtained:

$$R_q''(\beta) + \frac{1}{\tan\alpha} R_q'(\beta) - \frac{n^2}{\sin^2\alpha} R_q(\beta) = 0 \tag{44}$$

Solution of the above differential equation yields the following [26]:

$$R_q(\beta) = A\beta^n \left\{ 1 + \frac{n}{12}\beta^2 + \frac{(5n+7)n}{1440}\beta^4 + \frac{n(n+4)(5n+1)}{51840}\beta^6 \right\} \tag{45}$$

Finally, the hydrodynamic pressure, Eq. (40), in terms of velocity potential and radial displacement is written:

$$P_f = -\rho_f k \sum_{q=1}^{8} x \frac{\partial^2 W_q}{\partial t^2} \tag{46}$$

where

$$k = \frac{\alpha}{n}\left[ \frac{1 + \frac{n}{12}\alpha^2 + \frac{(5n+7)n}{1440}\alpha^4 + \frac{n(n+4)(5n+1)}{51840}\alpha^6}{1 + \frac{(n+2)}{12}\alpha^2 + \frac{(n+4)(5n+7)}{1440}\alpha^4 + \frac{(n+4)(n+6)(5n+1)}{51840}\alpha^6} \right] \tag{47}$$

By substituting the expression of $W$ given in Eq. (31) into this pressure relation, Eq. (46), and introducing the general force vector as was done in the previous section, the fluid mass matrix is obtained:

$$[m_f] = [A^{-1}]^{\mathrm{T}}[S_f][A^{-1}] \tag{48}$$

where

$$[S_f] = -\rho_f k \int \int x[N]^{\mathrm{T}}[N_w]\,\mathrm{d}A \tag{49}$$

The global fluid mass matrix $\mathbf{M_f}$ for the case that the shell is partially or completely filled with fluid is now entered into the governing equation.

## 4. Aeroelastic model

The governing equation of motion in a global system for a fluid-filled conical shell exposed to external supersonic airflow is described using the following relation:

$$[M_s - M_f]\{\ddot{\delta}\} - \rho_\infty U_\infty \frac{M^2-2}{(M^2-1)^{3/2}}[C_f]\{\dot{\delta}\} + \left[ [K_s] + [K_l] - \left( \frac{\rho_\infty U_\infty^2}{(M^2-1)^{1/2}}[K_{f_1}] - \frac{\rho_\infty U_\infty^2}{2(M^2-1)R_m}[K_{f_2}] \right) \right] \{\delta\} = 0 \tag{50}$$

where subscripts $s$ and $f$ refer to a shell in vacuo and fluid, respectively and $I$ refers to a shell under initial membrane forces (hydrostatic pressure and axial load). Assuming the oscillatory motion in the form $\{\delta\} = \delta_0 e^{i\omega t}$, eventually Eq. (50) leads to the eigenvalue problem where its eigenvalues occur in complex conjugates pairs. Aeroelastic stability of the shell is investigated by studying the eigenvalues in the complex plane. Flutter onset occurs when the imaginary part of the eigen frequencies $\omega$, change from positive to negative.

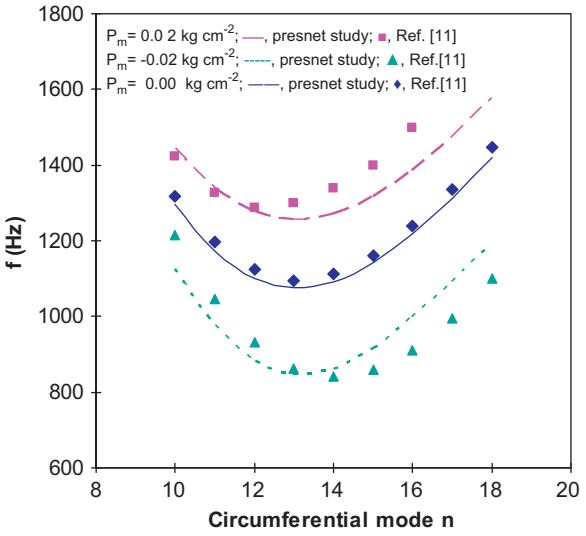


**Fig. 3.** Effect of pressure difference on natural frequency versus circumferential wave number.

## 5. Numerical results

### 5.1. Validation

Two different thin conical shells are treated here for validation. The first problem studies free vibration and buckling of a thin cone examined by Ueda and et al. [11]. Numerical calculation is carried out for the wind tunnel test model of a truncated conical shell made of super-Invar for which Young's modulus, Poisson's ratio and density are $1.28 \times 10^4$ kg mm$^{-2}$,

**Table 1**
Critical freestream dynamic pressure for the conical shell.

| Source | $\Lambda_{cr}$ | $n_{cr}$ |
|---|---|---|
| Shulman [10]: | 669 | 6 |
| Galerkin, 4 terms | | |
| Dixon and Hudson [12]: | | |
| Galerkin, 4 terms | 492 | 5 |
| Galerkin, 8 terms | 588 | 5 |
| Galerkin, 12 terms | 590 | 5 |
| Bismarck-Nasr [14], FEM: | 702 | 6 |
| Present study: | | |
| Pressure by Eq. (29) | 598 | 6 |
| Pressure by Eq. (30) | 628 | 6 |

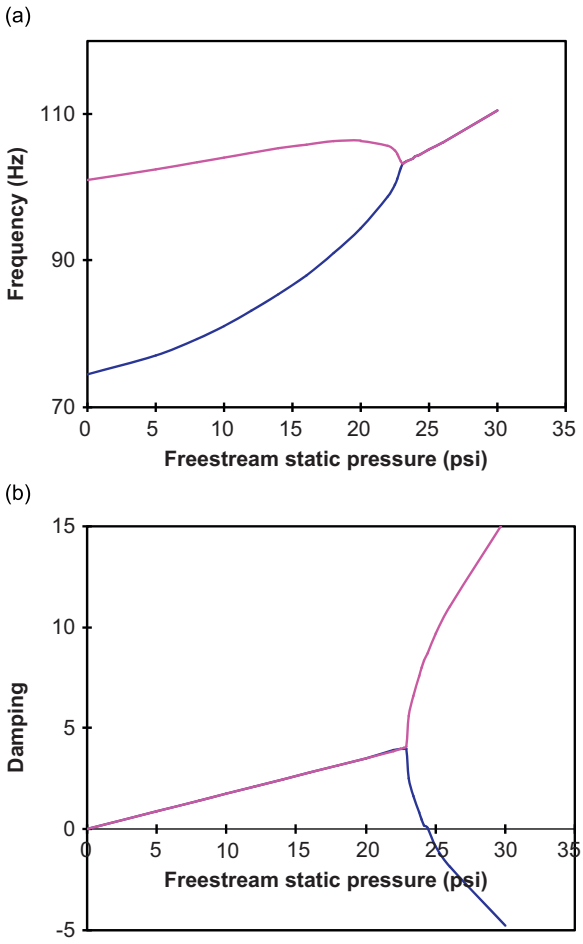


**Fig. 4.** (a) Real part and (b) imaginary part of the complex frequencies, $n$=6, versus freestream static pressure, aerodynamic pressure evaluated by Eq. (29).

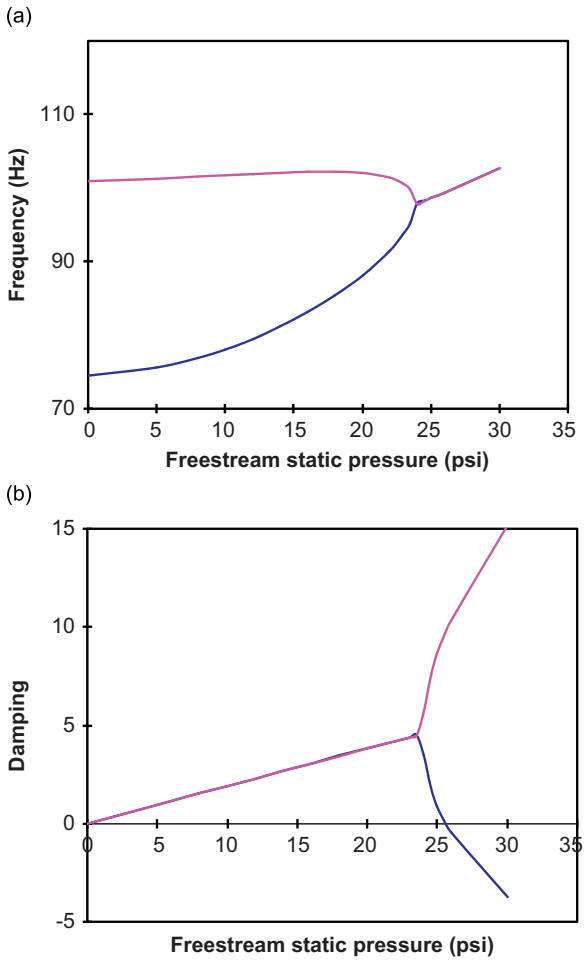


**Fig. 5.** (a) Real part and (b) imaginary part of the complex frequencies, $n$=6, versus freestream static pressure, aerodynamic pressure evaluated by Eq. (30).

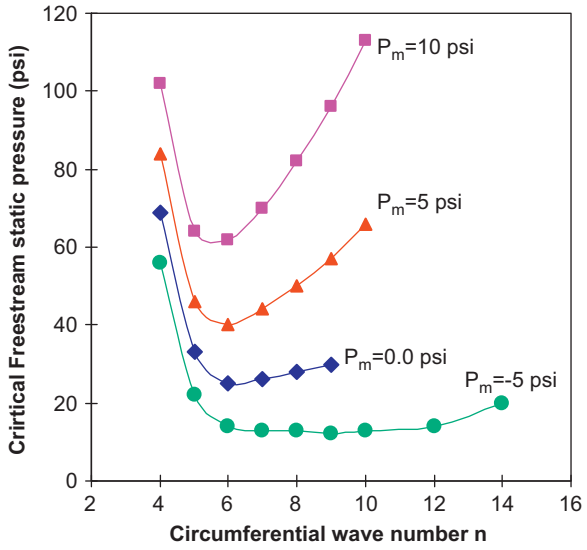


**Fig. 6.** Flutter boundaries for stressed shell. $R_1/h = 148$, $L/R_1 = 8.13$, $h = 0.051$ in, $\alpha = 5^{\circ}$, $P_x = 0.0$.

0.25 and $8.13 \times 10^{-10}$ kg s$^2$ mm$^{-4}$, respectively. The shell has a ratio of slant length to small radius of $L/R_1 = 1.61$, a semivertex angle of 14° and clamped edges. The effect of pressure difference on the natural frequency of the 0.05 mm thick shell is shown in Fig. 3. The positive value is due to the fact that the internal pressure makes the natural frequencies increase, in other words it has a stabilizing effect. External pressure, on the other hand, causes a decrease in the natural frequencies. These trends, which are calculated using only 15 elements show good agreement with the results obtained in Ref. [11]. For large values of external pressure the natural frequency becomes purely imaginary which represents the buckling state of the shell. The second problem treated for validation is the flutter boundary of a simply-supported cone subjected to external supersonic airflow. This case has been studied by various authors [10,12,14]. The shell has the following data: Young's modulus, $E = 6.5 \times 10^6$ lb in$^{-2}$, Poisson's ratio, $\upsilon = 0.29$, material mass density, $\rho = 8.33 \times 10^{-4}$ lb s$^2$ in$^{-4}$, shell thickness, $h = 0.051$ in, cone semivertex angle, $\alpha = 5^\circ$, small end radius to thickness, $R_1/h = 148$, and $L/R_1 = 8.13$ where $L$ is the shell length. The supersonic airflow has freestream Mach number, $M_\infty = 3$, stagnation temperature, $T_\infty = 288.15$ K and stagnation pressure, $P_{s\infty} = 14.696$ lb in$^{-2}$. The boundary conditions at both ends are $u$=$w$=$v$=0. In Table 1, the critical dynamic pressure parameter is defined:

$$\Lambda = \frac{\rho_\infty U^2 R_1^3}{K(M_\infty^2 - 1)^{1/2}} \tag{51}$$

where $k$ is expressed by Eq. (7). When results are summarized and compared with other finite element and analytical solutions, this method shows good convergence using only 15 elements with small disagreements. It should be noted that the previous analytical methods [10,12] use Donnell-Mushtari simplified shell theory while Ref. [14] uses Novozhilov's thin shell theory with the different method of application of finite element solution. These explain the small disagreement in the results of Table 1.

### 5.2. Flutter boundary

The conical shell of the preceding validation for flutter boundary is treated here. The complex frequencies only for the first and second modes versus free stream dynamic pressure are plotted in Fig. 4. Aerodynamic pressure is evaluated using

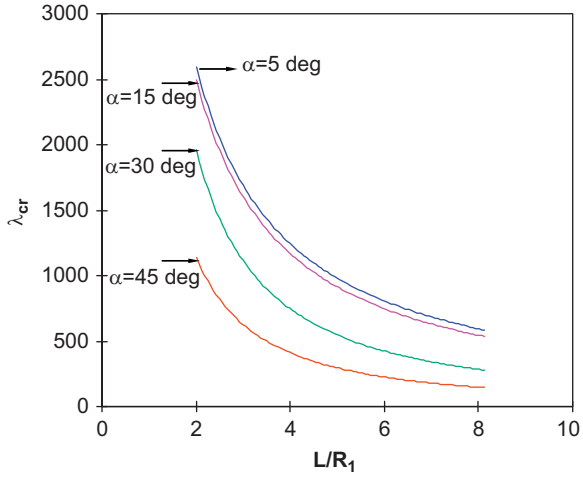


**Fig. 7.** Variation of critical dynamic pressure parameter, Eq. (51), with $L/R_1$, for an isotropic shell, $R_1/h = 148$, $5 \le \alpha \le 45$, $P_m = P_x = 0.0$, $u$=$v$=$w$=0.

**Table 2**
Critical freestream static pressure for different boundary conditions.

| Boundary condition | $p_\infty$ (psi) | Mode no. |
|---|---|---|
| Freely simply supported ($v$=$w$=0) | 27 | Coupled 1st and 2nd |
| Simply supported ($u$=$v$=$w$=0) | 24.5 | Coupled 1st and 2nd |
| Clamped-clamped | 24.5 | Coupled 1st and 2nd |
| Free–free | | |
| Divergence | 39 | 1st |
| Flutter | 45 | Coupled 3rd and 4th |

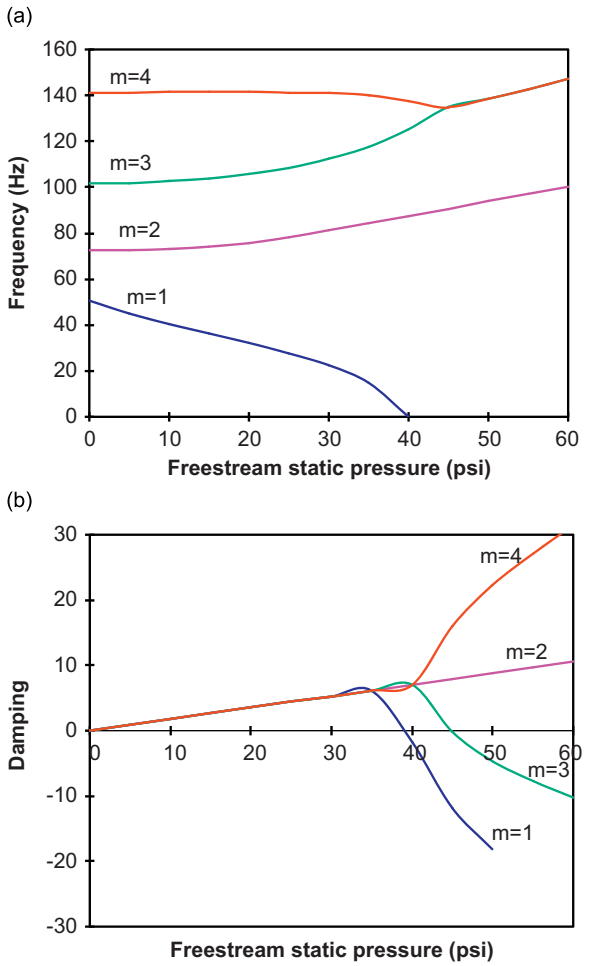


**Fig. 8.** (a) Real part and (b) imaginary part of the complex frequencies, $n$=6, versus freestream static pressure, aerodynamic pressure evaluated by Eq. (29).

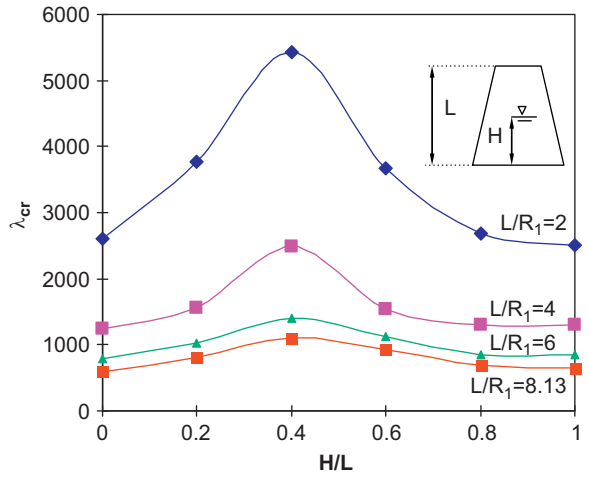


**Fig. 9.** Flutter boundary for different filling ratios $H/L$; $R_1/h = 148$, $\alpha = 5^{\circ}$.

Eq. (29). In Fig. 4a the real part of the complex frequency increases for the first mode while for the second mode it decreases as the freestream dynamic pressure increases. For higher values of dynamic pressure these real parts, representing the oscillation frequency, eventually coalesce into a single mode. Further increasing the dynamic pressure of flow causes the shell to lose its stability at $P_\infty = 24.8$ psi. This instability is due to coupled-mode flutter where the imaginary part of complex frequency (representing the damping of the system) crosses the zero value in Fig. 4b. The same behavior is observed in Fig. 5 but instability occurs at $p_\infty = 25.2$ psi where the aerodynamic pressure is evaluated using Eq. (30). For the shell treated here, one can see that the curvature term in the aerodynamic pressure expression has a small effect on the flutter boundary.

The flutter boundaries for different circumferential wave numbers for various shell internal or external pressures are reported in Fig. 6. Shell geometry and flow parameters are the same as used in the previous case study. When the shell is pressurized it becomes unstable at higher dynamic pressure levels due to an increase in stiffness because of applied internal pressure. External pressure decreases the stiffness of the shell which results in a lower critical freestream dynamic pressure.

In Fig. 7 the onset of flutter for different semivertex angles, $\alpha$, and different $L/R_1$ ratios is plotted. By increasing the conicity effect, flutter instability occurs at lower dynamic pressures for longer shells. This decrease in $\Lambda_{cr}$ with $\alpha$ is attributed to the fact that the natural frequencies always decrease with increasing the $L/R_1$ and $\alpha$.

The effect of boundary conditions on the flutter onset is presented in Table 2. It is seen that for freely simply-supported ends, $v$=$w$=0, flutter onset occurs at 27 psi which indicates more flutter resistance compared to simply support or clamped ends. It also indicated that there is no difference for flutter onset when the shell is either clamped or simply supported $u$=$v$=$w$=0 at the both ends. When the shell is free at both ends the instability is slightly different and two types of instability are observed. In Fig. 8a the real part of the complex frequency for the first mode decreases as the freestream static pressure increases, while the imaginary part remains positive. The existence of a zero real part and a negative imaginary part of the complex frequency indicates that the shell diverges statically. By further increasing the freestream static pressure, second mode remains stable but the real parts of third and forth modes merge into a single mode and their imaginary parts bifurcate into two branches and one of them becomes negative. At this point, $p_\infty = 45$ psi, the shell loses stability due to coupled-mode flutter because a negative imaginary part makes the vibration amplitude grow.

### 5.3. *Effect of filling ratio*

In this section the effect of filling ratio on the flutter boundary is investigated. Fig. 9 shows the critical value of freestream static pressure for different filling ratios, $H/L$, and for various lengths of the shell, $L/R_1$. Shell geometry and flow parameters are the same as the previous case study with liquid-filled density $\rho_f = 9.355 \times 10^{-5}$ lb s$^2$ in$^{-4}$. In general, the critical dynamic pressure parameter for an empty shell increases as the length ratio is decreased. It is seen that the value of critical dynamic pressure changes rapidly and widely as the filling ratio increases from a low value. In addition, by increasing the length ratio the decrement of the critical value of $\Lambda$ is decreased and vanishes when coupled-mode flutter type instability occurs. This rapid change in critical dynamic pressure at low filling ratios and its almost steady behaviour at large filling ratios indicates that the fluid near the bottom of the shell is largely influenced by elastic deformation when a shell is subjected to external subsonic flow.

## 6. Conclusion

An efficient hybrid finite element method is presented to analyze the aeroelastic stability of an empty or partially liquid-filled conical shell subjected to external supersonic flow. Sanders linear shell theory is coupled with first order piston theory to account for aerodynamic pressure. Fluid–structure interaction due to hydrodynamic pressure of an internal fluid along with the effects of initial stress stiffening is also taken into account. The study has been done for shells with various geometries and boundary conditions. In all study cases one type of instability is found; coupled-mode flutter in the first and second mode. For the free–free boundary condition however, the shell loses its stability first through divergence and then by flutter due to coupling of the third and forth modes. An internally pressurized shell shows more flutter resistance than a shell under external pressure. Decreasing the vertex angle of the cone causes the flutter boundary to occur at a lower dynamic pressure. A lower filling ratio has more flutter resistance for short shells than long shells. The proposed hybrid finite element package can present reliable results at less computational cost compared to commercial software since the latter imposes some restrictions when such an analysis is done.

## Acknowledgments

The authors acknowledge the financial support of NSERC of Canada, Grant no. A8814.

## Appendix A

The equilibrium equations (Eq. (4)) are:

$$L_1(x,\theta,B_{ij}) = B_{11}\left[2x\sin\alpha\frac{\partial U}{\partial x}+x^2\frac{\partial^2 U}{\partial x^2}\right]+B_{12}\left[x\frac{\partial^2 V}{\partial x\partial\theta}+x\cos\alpha\frac{\partial W}{\partial x}+U\sin\alpha+W\cos\alpha\right]-B_{14}\left[3x^2\sin\alpha\frac{\partial^2 W}{\partial x^2}+x^3\sin\alpha\frac{\partial^3 W}{\partial x^3}\right]$$
$$+B_{15}\left[x\cot\alpha\frac{\partial V}{\partial x\partial\theta}-\frac{x}{\sin\alpha}\frac{\partial^3 W}{\partial\theta^2\partial x}-2x\sin\alpha\frac{\partial W}{\partial x}-x^2\sin\alpha\frac{\partial^2 W}{\partial x^2}+\cot\alpha\frac{\partial V}{\partial\theta}-\frac{1}{\sin\alpha}\frac{\partial^2 W}{\partial\theta^2}\right]$$
$$-B_{22}\left[\frac{\partial V}{\partial\theta}+\sin\alpha U+\cos\alpha W\right]+B_{24}\left[x^2\sin\alpha\frac{\partial^2 W}{\partial x^2}\right]+B_{25}\left[-\cot\alpha\frac{\partial V}{\partial\theta}+\frac{1}{\sin\alpha}\frac{\partial^2 W}{\partial\theta^2}+x\sin\alpha\frac{\partial W}{\partial x}\right]$$
$$+B_{33}\left[x\frac{\partial^2 V}{\partial x\partial\theta}+\frac{1}{\sin\alpha}\frac{\partial^2 U}{\partial\theta^2}-\frac{\partial V}{\partial\theta}\right]+B_{36}\left[-\frac{2x}{\sin\alpha}\frac{\partial^3 W}{\partial\theta^2\partial x}+x\cot\alpha\frac{\partial^2 V}{\partial x\partial\theta}-\frac{\cot\alpha}{\sin\alpha}\frac{\partial^2 U}{\partial\theta^2}+\frac{2}{\sin\alpha}\frac{\partial^2 W}{\partial\theta^2}-\cot\alpha\frac{\partial V}{\partial\theta}\right]$$
$$+B_{66}\left[\frac{x\cot\alpha}{\sin\alpha}\frac{\partial^3 W}{\partial\theta^2\partial x}-\frac{3x}{4}\cot^2\alpha\frac{\partial^2 V}{\partial x\partial\theta}+\frac{\cot^2\alpha}{4\sin\alpha}\frac{\partial^2 U}{\partial\theta^2}-\frac{\cot\alpha}{\sin\alpha}\frac{\partial^2 W}{\partial\theta^2}+\frac{3\cot^2\alpha}{4}\frac{\partial V}{\partial\theta}\right]$$

$$L_2(x,\theta,B_{ij}) = B_{12}x\frac{\partial^2 U}{\partial x\partial\theta}+B_{15}x\cot\alpha\frac{\partial^2 U}{\partial x\partial\theta}+B_{22}\left[\frac{1}{\sin\alpha}\frac{\partial^2 V}{\partial\theta^2}+\frac{\partial U}{\partial\theta}+\cot\alpha\frac{\partial W}{\partial\theta}\right]-B_{24}x^2\frac{\partial^3 W}{\partial x^2\partial\theta}$$
$$+B_{25}\left[\frac{2\cot\alpha}{\sin\alpha}\frac{\partial^2 V}{\partial\theta^2}-\frac{1}{\sin^2\alpha}\frac{\partial^3 W}{\partial\theta^3}-x\frac{\partial^2 W}{\partial x\partial\theta}+\cot^2\alpha\frac{\partial W}{\partial\theta}+\cot\alpha\frac{\partial U}{\partial\theta}\right]-B_{45}x^2\cot\alpha\frac{\partial^3 W}{\partial x^2\partial\theta}$$
$$+B_{55}\left[\frac{\cot^2\alpha}{\sin\alpha}\frac{\partial^2 V}{\partial\theta^2}-\frac{\cot\alpha}{\sin^2\alpha}\frac{\partial^3 W}{\partial\theta^3}-x\cot\frac{\partial^2 W}{\partial x\partial\theta}\right]$$
$$B_{33}\left[x^2\sin\alpha\frac{\partial^2 V}{\partial x^2}+x\cot\alpha\frac{\partial^2 U}{\partial x\partial\theta}-4x\frac{\partial^2 W}{\partial x\partial\theta}+6x\cos\alpha\frac{\partial V}{\partial x}+2\cot\alpha\frac{\partial U}{\partial\theta}+4\frac{\partial W}{\partial\theta}-6\cos\alpha V\right]$$
$$+B_{66}\left[\begin{array}{c}-6x\cot\alpha\frac{\partial^2 W}{\partial x\partial\theta}-3x^2\cot\alpha\frac{\partial^3 W}{\partial x^2\partial\theta}+\frac{9x}{2}\cos\alpha\cot\alpha\frac{\partial V}{\partial x}+\frac{9x^2}{4}\cos\alpha\cot\alpha\frac{\partial^2 V}{\partial x^2}-\frac{3}{2}\cot^2\alpha\frac{\partial U}{\partial\theta}\\ -\frac{3x}{4}\cot^2\alpha\frac{\partial^2 U}{\partial x\partial\theta}+6\cot\alpha\frac{\partial W}{\partial\theta}-\frac{9}{2}\cos\alpha\cot\alpha V\end{array}\right]$$

$$L_3(x,\theta,B_{ij}) = -B_{12}x\cos\alpha\frac{\partial U}{\partial x}+B_{14}\left[6x\sin\alpha\frac{\partial U}{\partial x}+6x^2\sin\alpha\frac{\partial^2 U}{\partial x^2}+x^3\sin\alpha\frac{\partial^3 U}{\partial x^3}\right]$$
$$+B_{15}\left[\frac{x}{\sin\alpha}\frac{\partial^3 U}{\partial\theta^2\partial x}-2x\sin\alpha\frac{\partial U}{\partial x}-x^2\sin\alpha\frac{\partial^2 U}{\partial x^2}\right]-B_{22}\left[\cot\alpha\frac{\partial V}{\partial\theta}+\cos\alpha U+\cos\alpha\cot\alpha W\right]$$
$$+B_{24}\left[4x\frac{\partial^2 V}{\partial x\partial\theta}+x^2\frac{\partial^3 V}{\partial x^2\partial\theta}+4x\sin\alpha\frac{\partial U}{\partial x}+x^2\sin\alpha\frac{\partial^2 U}{\partial x^2}\right.$$
$$\left.+4x\cos\alpha\frac{\partial W}{\partial x}+2x^2\cos\alpha\frac{\partial^2 W}{\partial x^2}+2\frac{\partial V}{\partial\theta}+2\sin\alpha U+2\cos\alpha W\right]$$
$$+B_{25}\left[-\cot^2\alpha\frac{\partial V}{\partial\theta}+\frac{1}{\sin^2\alpha}\frac{\partial^3 V}{\partial\theta^3}+\frac{1}{\sin\alpha}\frac{\partial^2 U}{\partial\theta^2}+2\frac{\cot\alpha}{\sin\alpha}\frac{\partial^2 W}{\partial\theta^2}-\frac{\partial V}{\partial\theta}-x\frac{\partial^2 V}{\partial x\partial\theta}\right.$$
$$\left.-\sin\alpha U-x\sin\alpha\frac{\partial U}{\partial x}-\cos\alpha W\right]$$
$$+B_{36}\left[6x\frac{\partial^2 V}{\partial x\partial\theta}+2x^2\frac{\partial^3 V}{\partial x^2\partial\theta}+\frac{4}{\sin\alpha}\frac{\partial^2 U}{\partial\theta^2}+\frac{2x}{\sin\alpha}\frac{\partial^3 U}{\partial\theta^2\partial x}-4\frac{\partial V}{\partial\theta}-2x\frac{\partial^2 V}{\partial x\partial\theta}\right]$$
$$-B_{44}\left[12x^2\sin\alpha\frac{\partial^2 W}{\partial x^2}+8x^3\sin\alpha\frac{\partial^3 W}{\partial x^3}+x^4\sin\alpha\frac{\partial^4 W}{\partial x^4}\right]$$
$$+B_{45}\left[4x\cot\alpha\frac{\partial^2 V}{\partial x\partial\theta}+x^2\cot\alpha\frac{\partial^3 V}{\partial x^2\partial\theta}-\frac{4x}{\sin\alpha}\frac{\partial^3 W}{\partial x\partial\theta^2}-\frac{2x^2}{\sin\alpha}\frac{\partial^4 W}{\partial\theta^2\partial^2 x}\right.$$
$$\left.-6x\sin\alpha\frac{\partial W}{\partial x}+2\cot\alpha\frac{\partial V}{\partial\theta}-\frac{2}{\sin\alpha}\frac{\partial^2 W}{\partial\theta^2}-3x^2\sin\alpha\frac{\partial^2 W}{\partial x^2}\right]$$

$$-B_{55}\left[\cot\alpha\frac{\partial V}{\partial\theta}+x\cot\alpha\frac{\partial^2 V}{\partial x\partial\theta}-\frac{1}{\sin\alpha}\frac{\partial^2 W}{\partial\theta^2}-2x\sin\alpha\frac{\partial^2 W}{\partial x^2}-x^2\sin\alpha\frac{\partial^2 W}{\partial x^2}\right.$$
$$\left.-\frac{\cot\alpha}{\sin^2\alpha}\frac{\partial^3 V}{\partial\theta^3}+\frac{1}{\sin^3\alpha}\frac{\partial^4 W}{\partial\theta^4}\right]+B_{66}\left[-\frac{8x}{\sin\alpha}\frac{\partial^3 W}{\partial\theta^2\partial x}-\frac{4x^2}{\sin\alpha}\frac{\partial^4 W}{\partial\theta^2\partial x^2}+6x\cot\alpha\frac{\partial^2 V}{\partial x\partial\theta}\right.$$
$$\left.+3x^2\cot\alpha\frac{\partial^3 V}{\partial x^2\partial\theta}-\frac{2\cot\alpha}{\sin\alpha}\frac{\partial^2 U}{\partial\theta^2}-\frac{x\cot\alpha}{\sin\alpha}\frac{\partial^3 U}{\partial\theta^2\partial x}+\frac{8}{\sin\alpha}\frac{\partial^2 W}{\partial\theta^2}-6\cot\alpha\frac{\partial V}{\partial\theta}\right] \quad \text{(A1)}$$

## References


[1] M.N. Bismarck-Nasr, Finite elements in aeroelasticity of plates and shells, *Applied Mechanics Reviews* 49 (1996) 17–24.
[2] E.H. Dowell, *Aeroelasticity of Plates and Shells*, Noordhoff International Publishing, Leyden, 1975.
[3] M.D. Olson, Y.C. Fung, Supersonic flutter of circular cylindrical shells subjected to internal pressure and axial compression, *AIAA Journal* 4 (1966) 858–864.
[4] M.D. Olson, Y.C. Fung, Comparing theory and experiment for supersonic flutter of circular cylindrical shells, *AIAA Journal* 5 (1967) 1849–1856.
[5] G.W. Barr, R.O. Stearman, Aeroelastic stability characteristics of cylindrical shells considering imperfections and edge constraint, *AIAA Journal* 7 (1969) 912–919.
[6] M.N. Bismarck-Nasr, Finite element method applied to the supersonic flutter of circular cylindrical shells, *International Journal for Numerical Methods in Engineering* 10 (1976) 423–435.
[7] M. Ganapathi, T.K. Varadan, J. Jijen, Field-consistent element applied to clutter analysis of circular cylindrical shells, *Journal of Sound and Vibration* 171 (1994) 509–527.
[8] M. Amabili, F. Pellicano, Nonlinear supersonic flutter of circular cylindrical shells, *AIAA Journal* 39 (2001) 564–573.
[9] M. Amabili, F. Pellicano, Multimode approach to nonlinear supersonic flutter of imperfect circular cylindrical shells, *Journal of Applied Mechanics, Transactions ASME* 69 (2002) 117–129.
[10] Y. Shulman, Vibration and flutter of cylindrical and conical shells. MIT ASRL Rept. 74-2 OSR Tech. Rept. 59-776, 1959.
[11] T. Ueda, S. Kobayashi, M. Kihira, Supersonic flutter of truncated conical shells, *Transactions of the Japan Society for Aeronautical and Space Sciences* 20 (1977) 13–30.
[12] S.C. Dixon, M.L. Hudson, Flutter, vibration, and buckling of truncated orthotropic conical shells with generalized elastic edge restraint. NASA TN D-5759, 1970.
[13] R. Miserentino, S.C. Dixon, Vibration and flutter tests of a pressurized thin-walled truncated conical shell. NASA TN D-6106, 1971.
[14] M.N. Bismarck-Nasr, H.R. Costa Savio, Finite-element solution of the supersonic flutter of conical shells, *AIAA Journal* 17 (1979) 1148–1150.
[15] P.J. Sunder, V.C. Ramakrishnan, S. Sengupta, Finite element analysis of 3-ply laminated conical shell for flutter, *International Journal for Numerical Methods in Engineering* 19 (1983) 1183–1192.
[16] P.J. Sunder, V.C. Ramakrishnan, S. Sengupta, Optimum cone angles in aeroelastic flutter, *Computer & Structures* 17 (1983) 25–29.
[17] D.R. Mason, P.T. Blotter, Finite-element application to rocket nozzle aeroelasticity, *Journal of Propulsion and Power* 2 (1986) 499–507.
[18] A.A. Lakis, P. Van Dyke, H. Ouriche, Dynamic analysis of anisotropic fluid-filled conical shells, *Journal of Fluid and Structures* 6 (1992) 135–162.
[19] S.D. Kumar, N. Ganesan, Dynamic analysis of conical shells conveying fluid, *Journal of Sound and Vibration* 310 (2008) 38–57.
[20] A.A. Lakis, M.P. Paidoussis, Dynamic analysis of axially non-uniform thin cylindrical shells, *Journal of Mechanical Engineering Science* 14 (1972) 49–71.
[21] J.L. Sanders, An improved first-approximation theory for thin shell. NASA R-24, 1959.
[22] W. Flugge, second ed., *Stress in Shell*Springer-verlag, 1973.
[23] O.C. Zienkiewicz, R.L. Taylor, fifth ed., *The Finite Element Method Volume:2 Solid Mechanics*Butterworht-Heinemann, Oxford, 2000.
[24] R.H. MacNeal, Nastran theoretical manual. NASA SP-221, 1972.
[25] H. Ashley, G. Zartarian, Piston theory-new aerodynamic tool for aeroelastician, *Journal of the Aeronautical Sciences* 23 (1956) 1109–1118.
[26] G.A. Korn, T.M. Korn, *Mathematical Handbook for Scientists and Engineer*, second ed., McGraw-Hill, New York, 1968.